Check for updates

[Palaeontology, Vol. 63, Part 4, 2020, pp. 651-660]

SILICA ENTRY AND ACCUMULATION IN STANDING TREES IN A HOT-SPRING ENVIRONMENT: CELLULAR PATHWAYS, RAPID PACE AND FOSSILIZATION POTENTIAL

by MORITZ LIESEGANG D and CAROLE T. GEE

Division of Palaeontology, Institute of Geosciences, Nussallee 8, 53115, Bonn, Germany; m.liesegang@uni-bonn.de, cgee@uni-bonn.de

Typescript received 10 August 2019; accepted in revised form 10 February 2020

Abstract: Silicification is the most important process of fossilization resulting in the preservation of internal tissues in plants, thereby providing essential information on the anatomy, life history, and evolution of land plants. However, fundamental knowledge of silica uptake, precipitation, and contribution to in situ plant fossilization is limited. To identify the cellular pathway of aqueous silica and subsequent fluid-wood interaction processes, we investigated upright standing young trees of lodgepole pine (Pinus contorta) in the hot-spring environment of Cistern Spring, Yellowstone National Park, USA. Our multi-method analytical approach using x-ray diffraction, Raman spectroscopy, scanning electron microscopy, and electron probe microanalyses shows that the surficial and internally co-precipitated silica-halitegypsum assemblage traces the flow of silica-rich fluid and documents fluid retention after short-term hot-spring water immersion and evaporation. Element distribution maps

reveal systematic 2D and 3D differences between silica quantities deposited in earlywood and latewood. The distribution of inorganic impurities in cell walls traces the anatomical structure of the wood and indicates rapid migration of homogeneous fluid into the waterlogged organic substrate. Our results show that the preferential pathway of silica-rich fluid into the above-ground wood was through the decorticated periphery which took place during a short-term flooding, ranging from days to weeks, of hot-spring fluid. In conclusion, the fluid retention capability in cellular pore space controls the *in situ* silicification process. The silicification of trees in growth position is a rapid process in which the *in vivo* transport of silica-rich fluid upward through the secondary xylem plays an insignificant role.

Key words: hot springs, *Pinus contorta*, *in situ* fossilization, silica, taphonomy, wood.

SINCE the terrestrialization of Earth by vascular plants in the middle Palaeozoic, silicification has played a major role in palaeobotanical fossilization. The best known silicified material comes from the Early Devonian Rhynie chert in Scotland, in which early land plants are exquisitely preserved in three dimensions on the cellular level (Edwards et al. 2017 and references therein). Here, small plants, animals and fungi are found in a chert, mineralized in place as they lived in a microhabitat at the margins of the sinter apron of a 407 million year old hot spring. Soon afterwards, in the Middle and Late Devonian, silicified arborescent plants show up in the palaeontological record. The ancient trees of Cladoxylopsida ferns (Xu et al. 2017) and progymnosperms such as Archaeopteris (Beck 1960) were able to achieve their large diameters and great heights through secondary growth and the production of wood. Since these trees are not entombed

in a silica-cemented sediment, for the trees to have become mineralized the plant bodies themselves must have selectively extracted silica from the silica-rich fluid percolating through the sediment. It is clear that in these cases, the silica precipitation reaction was spaciously specific, bonding preferentially to the inner cell walls of wood and permeating the wood cell walls. Hence, since the Devonian, the silicification of plants, and in particular of woody plants, has been facilitated by the natural affinity of secondary cell walls to aqueous silica. Specifically, it is thought that it results from the attraction of silicic acid to the ligno-holocellulosic complex of cell walls (Jefferson 1987; Ballhaus *et al.* 2012) on the reaction surface of the secondary cell wall.

Indeed, understanding the chemistry behind wood silicification has been a topic of interest among palaeobotanists and mineralogists since the 1940s (Murata 1940).

© 2020 The Authors.

doi: 10.1111/pala.12480

651

Palaeontology published by John Wiley & Sons Ltd on behalf of The Palaeontological Association

Since then, the introduction of new analytical techniques such as electron probe microanalysis, Raman spectroscopy and cathodoluminescence have contributed to a better understanding of the chemical and structural nature of the crystalline end-product quartz of the silicification process in wood (e.g. Sigleo 1978; Hellawell et al. 2015; Trümper et al. 2018). This in-depth understanding benefits substantially from the extensive knowledge gained from decades of studies of natural and synthetic silica (e.g. Jones & Segnit 1971; Iler 1979; Graetsch 1994; Götze et al. 2001; Rodgers et al. 2004; Liesegang et al. 2017). However, few studies have approached the issue of the early stages of the silicification process in wood, despite its fundamental importance for the diagenetic pathway and preservation potential of wood in the fossil record. Little is known about the entrance of aqueous silica into tree, whether through the roots or the trunk periphery, or both, or about the timing and characterization of the minerals involved in the fossilization process. One recent study targeting the entrance of aqueous silica into wood was carried out on a conifer twig found lying on the sinter apron of Cistern Spring, a hot spring in Yellowstone National Park, in which two cellular pathways were identified (Hellawell et al. 2015). Mineralogical analysis using electron probe microanalysis showed that the major entry of aqueous silica into the twig was through its periphery. A second entryway seemed to be through the roots of the tree, for there was greater silica accumulation in the earlywood than in the latewood of the growth rings of the twig. Yet, since this twig was not found in original growth position on a tree, but instead immersed in the silica-rich water of the sinter apron, the results from this study were not as conclusive as wood extracted from a tree in original growth position would have been.

We tackle here the questions regarding silica uptake and entry into upright trees rooted on a silica-rich substrate, as well as those on the patterns of silica deposition within the plant tissues. Do the trees take up silica with ground water through their roots? If this is the case, is there differential uptake, and hence greater amounts of silica deposition, in the earlywood relative to the latewood, as was found in the sinter apron twig from Cistern Spring (Hellawell et al. 2015)? Or, does silica preferentially accumulate in the rays or periphery of the woody stem? Further issues concern the composition of the mineral precipitates, the rate at which silicification occurs, and whether or not a tree will continue to take up and precipitate silica until its conducting cells are solidly mineralized, thus obstructing or even shutting down water transport in its vascular system.

Here we document incipient silicification in young trees that grew on a siliceous substrate in a hydrothermal setting, as well as trace the cellular pathway of aqueous silica and other minerals into the trunks of young upright trees. Our data consist of not only field observations, but also extensive high-resolution mineralogical analysis using scanning electron microscopy, electron probe microanalysis, confocal high-resolution Raman spectroscopy and x-ray powder diffraction. To the best of our knowledge, this study provides the first analysis of *in situ* conifer tree silicification in a modern hot-spring setting.

MATERIAL AND METHOD

Sampling

Wood specimens from four slender sapling trees of lodgepole pine (*Pinus contorta* var. *latifolia* (Engelmann) Critchfield; Fig. 1) were collected from a wide, flat area, about 10 m west of the pool margin of Cistern Spring in the Back Basin area of Norris Geyser Basin, Yellowstone National Park, Wyoming, USA. The saplings were sampled in an area of c. 9 m² that consists of dead standing trees of varying heights and girths. The ground between trees was barren of grass or other herbaceous plants.

In Yellowstone National Park, it is estimated that *Pinus contorta* is by far the most common species of plant in the park and comprises 80% of the forests (Waller *et al.* 2019). Lodgepole pine forest also dominates the vegetation around the Cistern Spring hot spring. These forests contain some patches of dead trees still rooted in growth position, which were probably killed during periodic, erratic outflows of the hot spring into the forest vegetation. In particular, the young trees of lodgepole pine found upright in original growth position on the silicarich substrate lent themselves best to our sampling and mineralogical analysis.

All saplings sampled ranged in age from 4 to 7 years old. They were dead, leafless, and decorticated, but still rooted in original growth position when collected. All four saplings were covered with a white coating along the lower portion of their trunks. The first tree (specimen YLP-1) was c. 0.81 m in height and observed as standing in a rivulet of Cistern Spring. In this case, nearly the entire trunk, a length of 0.78 m, was sampled. The second tree (specimen YLP-2) was c. 0.70 m in height and was growing on a dry, needle-covered patch of ground. The top 0.4 m of this tree was sampled. In both cases, the white coating appeared to be absent in the distal portions of the tree trunk. For comparison, samples of two other trees (YLP-3, YLP-4) were collected. The trees had heights of c. 1.95 m (YLP-3) and 1.57 m (YLP-4). Wood specimens from these trees were taken at c. 1 m above ground. Neither of these specimens had any observable white surface coating.

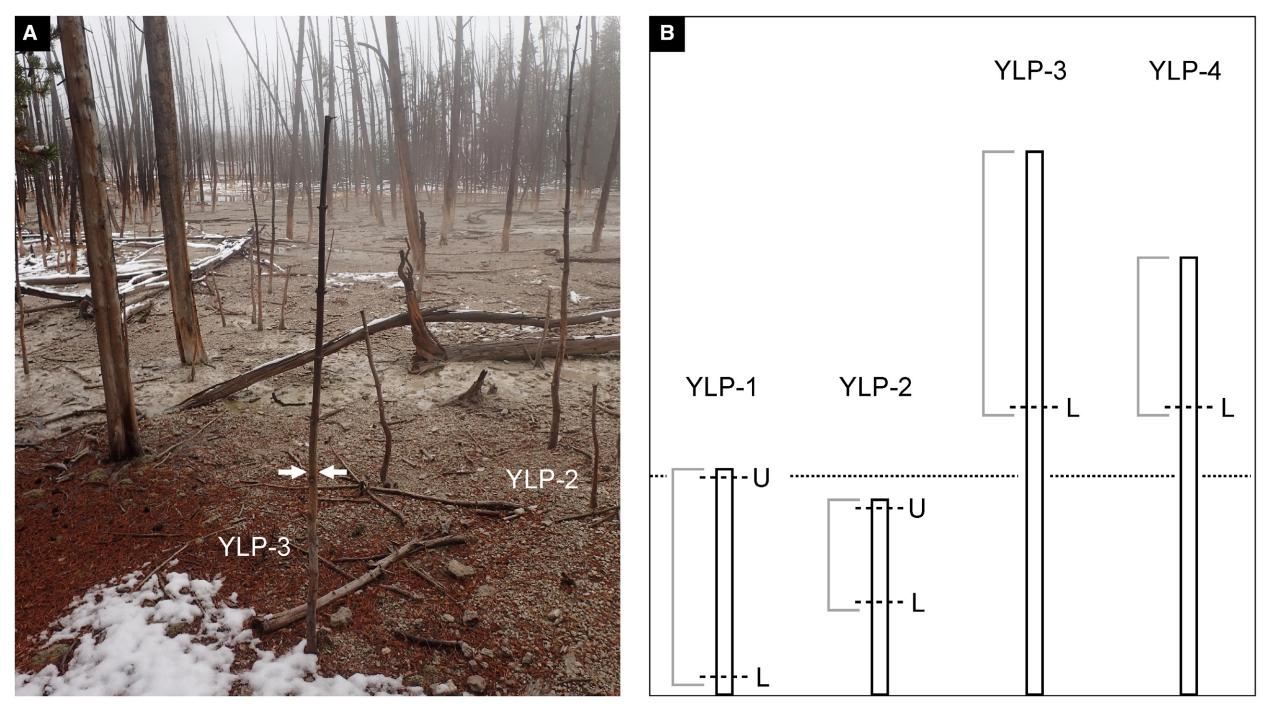


FIG. 1. Collecting information. A, locality showing two saplings; arrows mark height of white surface coating. B, schematic drawing of relative sapling height; dashed line represents height of white surface coating, brackets indicate specimens collected, U is upper cross section, L is lower cross section. Colour online.

Samples for analysis in the laboratory were cut from the lower portions of all four wood specimens, either as freshly fractured pieces of wood or as cut and polished transverse sections. A second set of samples for analysis was taken from each YLP-1 and YLP-2 near the top of the specimens.

Analytical methods

For high-resolution identification and characterization of the organic and inorganic compounds in the wood, the following analytical methods were applied: scanning electron microscopy (SEM), electron probe microanalysis (EPMA), confocal high-resolution Raman spectroscopy (CHRS), and x-ray powder diffraction analysis (XRPD).

The micromorphology of precipitated silica and its accompanying minerals was investigated using SEM on epoxy-embedded polished sections and the surfaces of freshly fractured material. To investigate the inner cells of the saplings in radial section, great care was taken to obtain fresh, cleanly fractured surfaces by taking samples from deep within the trunk to avoid contamination from the desiccation cracks on the outer surface of the tree. Fractured samples were then sputter-coated with c. 15 nm gold. Scanning electron images were made of the wood samples using a CamScan MV 2300 operated at an acceleration voltage of 20 kV and beam current of 55 nA.

Cross sections of the wood samples were epoxyembedded, dry-polished with corundum powder, and carbon-coated for EPMA and backscattered electron imaging. A JEOL JXA 8200 Superprobe, operated at an acceleration voltage of 15 kV and 15 nA beam current, was used to determine the silica spatial distribution and chemical composition. Each sample was analysed for SiO₂, TiO₂, Al₂O₃, Fe₂O_{3-total}, MgO, CaO, Na₂O, K₂O, and Cl. The acquisition time for Na analysis was 5 s on the peak and on the background, while peak and background of other elements were measured for 10 s each. Semi-quantitative compositional mapping was obtained using the wavelength-dispersive (WDS) detectors. Operating conditions were 15 kV acceleration voltage and 15 nA beam current, with a beam diameter of 1 µm and 60 ms counting time per 1-15 µm pixel size. The instrument was calibrated internally using synthetic/natural silicate and oxide.

Raman spectroscopy analyses of silica precipitates inside and on the outside of the saplings were conducted on a confocal Horiba Jobin Yvon LabRAM HR 800 spectrometer coupled to an Olympus BX41 microscope. A 785 nm air-cooled diode laser was used to excite the sample with a 100× objective (numerical aperture 0.9), a spectral integration time of 5 s, and 20 accumulations.

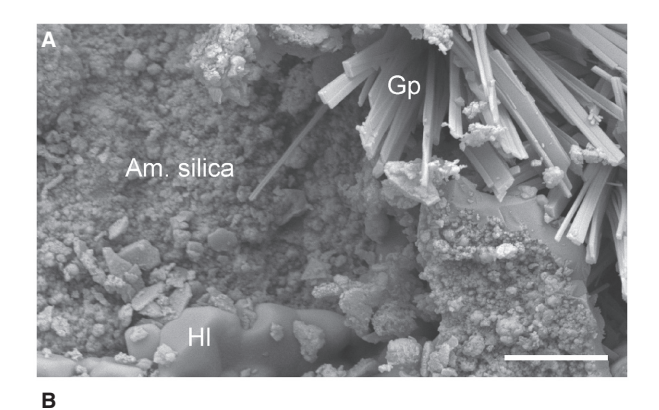
Scattered Raman light was collected in backscattering geometry and dispersed by a grating of 600 grooves/mm after passing through a 100 μm entrance slit. The confocal hole size was set to 1000 μm . Unpolarized spectra were collected with the Labspec 6 software at a spectral resolution of about 3.5/cm. An internal intensity correction (ICS, Horiba) was used to correct detector intensities. The instrument was calibrated using the Raman band of a silicon wafer at 520.7 cm $^{-1}$.

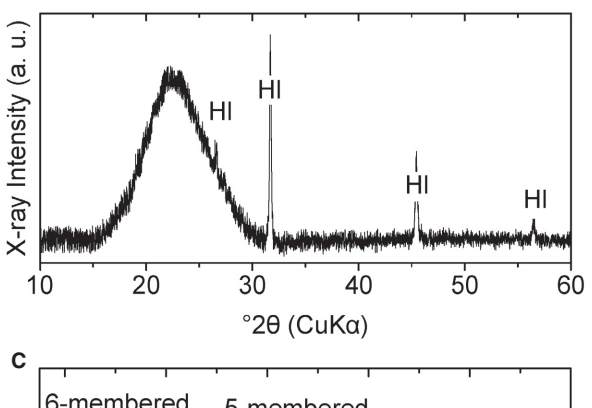
X-ray powder diffraction (XRPD) was carried out on the white surface precipitate scraped off the trunk specimens. The XRPD data was recorded on a PANalytical Empyrean diffractometer using CuK α radiation ($\lambda=1.5406~\mbox{Å})$ at 40 kV and a tube current of 40 mA. Powders were deposited in the depression of a Si single crystal and evenly distributed with a drop of ethanol that evaporated before measurements. Quartz powder (Merck Art.7536) was used as reference material.

RESULTS

Dead trees of lodgepole pine are omnipresent in the immediate vicinity of Cistern Spring hot spring in Yellowstone National Park. On the external surface of two white-coated saplings, YLP-1 and YLP-2, the white layer evenly blankets the outer surface of the barkless trunks, covering desiccation cracks and insect boreholes. This white coating consists of aggregates of silica spheres ranging from c. 150 to 450 nm and euhedral halite cubes (<10 μm) (Fig. 2A). The presence of minor acicular gypsum was confirmed by EDS and SEM analysis. The thickness of the coating is greatest at the lower end (c. 0.08 m height) of the trunk of YLP-1, measuring c. 700 µm, and gradually decreases to tens of micrometres at its apex (c. 0.8 m height). The thickness of the coating at the lower end of the trunk of YLP-2 measures c. 300 µm (c. 0.4 m height), and gradually decreases to tens of micrometres toward its apex (c. 0.7 m height) as well. A corresponding decrease in Si is reflected in the amount of silica that can be observed inside the wood cells, from the bottom to the top of the trunks.

X-ray powder diffraction and Raman spectroscopy identified the mineralogy of the surface coating and internally precipitated silica. The white surface coating, for example, shows a diffraction pattern with a broad, major asymmetric peak (Fig. 2B). This major peak at a maximum at $22.55^{\circ}2\theta$ (3.94 Å) is consistent with immature non-crystalline silica (opal-A) (see Rodgers *et al.* 2004; Liesegang *et al.* 2018), whereas the sharp intense peaks indicate halite. The white surface coating on the trunks YLP-1 and YLP-2 was confirmed as non-crystalline silica by confocal Raman spectroscopy. Figure 2C shows a Raman spectrum characteristic of the silica precipitates





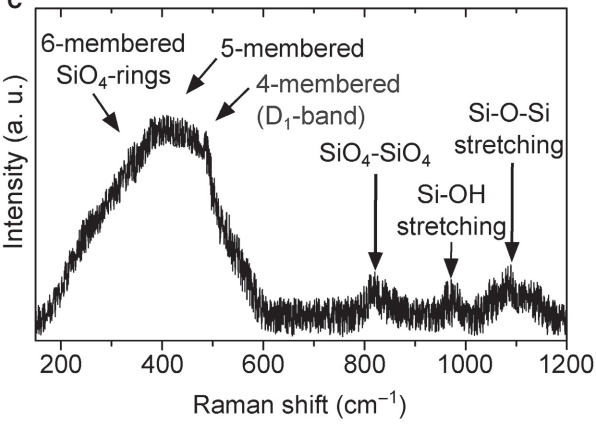


FIG. 2. A, secondary electron micrograph of the white surface coating; non-uniform spheres of amorphous silica (Am. silica), halite (HI) and acicular gypsum (Gp) on the base surface of YLP-1; scale bar represents 10 μ m. B, a representative x-ray diffractogram of the white surface coating from YLP-2 shows a broad peak centred at 22.55°2 θ (CuK α) (3.94 Å) indicative of amorphous silica (Liesegang *et al.* 2018); sharper peaks at larger 2 θ angles are attributed to halite (HI). C, a representative Raman spectrum of amorphous silica precipitates in the woody axis of YLP-1; band assignments are based on previous studies on vitreous silica (McMillan 1984).

on the sapling surfaces, as well as inside the tracheids. Among the samples, the spectra are identical and display a prominent broad band centred at 420 cm⁻¹ with a sharp D₁-band at 490 cm⁻¹. Broad bands of lower intensity are located at 815, 975, and 1086 cm⁻¹. The spectra

are generally consistent with those of opal-A and silica gel (see Hellawell et al. 2015; Liesegang & Milke 2018). Point analyses and line scans confirm the absence of other silica phases on the surface and inside the saplings.

SEM images of precipitated mineral phases reveal systematic variations of the silica micromorphology and spatial distribution that document the physico-chemical evolution of the silicifying fluids (Figs 3, 4E-F). A dense, continuous layer of amorphous silica lines the tracheid lumina, parenchyma rays, and circular bordered pit chambers in the lower sections of the white-coated trunks of YLP-1 and YLP-2 (Fig. 4E, F). This layer varies in thickness, ranging from c. 300 nm in earlywood lumina (Fig. 4E) to occasionally up to c. 800 nm in latewood lumina (Fig. 4F). Silica spheres of varying sizes (150-350 nm in diameter, mean 200 nm) are located on the surface of the dense layers of amorphous silica (Fig. 3A, B) and are found directly on and between the margo strands of the circular bordered pits (Fig. 3C). The range in size distribution of the silica spheres is uniform throughout the white-coated specimens and hence, is not related to their vertical position in the trunk (Fig. 3D). In the circular bordered pits of apex cross sections, only a few silica spheres can be observed between margo strands (Fig. 3E). Euhedral halite crystals up to 6 µm in size commonly fill the tracheid lumina and pit chambers of the circular bordered pits (Fig. 3F), as well as locally penetrating cell walls.

EPMA distribution mapping for silicon in the sections from the white-coated trunks of YLP-1 and YLP-2 shows clearly that silica has accumulated in the cell walls and lumina of tracheid wood cells (Fig. 4A, B). Silicon, along with other elements such as Na and Cl, is distributed throughout the trunk wood in cross section; EPMA maps of these elements highlight the cell walls of the tracheids (Fig. 4C-F). Silica is preferentially enriched in the parenchyma cells of the rays, in the latewood tracheids, and along the trunk periphery (Fig. 4A-C). Conversely, the lignin-rich middle lamella between cells is not enriched by silica or other elements (Fig. 4C, D).

In cross sections higher up in the trees, it can be observed that silica has also been deposited in the wood cells, although to a lesser extent than in the lower sections (Fig. 4A, B). As before, the silica accumulation is greatest along the periphery of the trunk and in the rays. In the upper section of sample YLP-1, which was sampled 0.66 m above the lower section, there is little silica accumulation in the tracheids of the inner wood, and the growth rings do not show up as distinctly as in the lower section, indicating little accumulation of other elements. In the upper cross sections, any difference in silica quantity between the earlywood and latewood is virtually absent in the uppermost sections because of the general lack of silica deposition at the top of the trunks (Fig. 4B).

Here, silica precipitates are restricted to desiccation cracks, the outermost part of the trunk, and rays; indeed, they are present in low quantities close to the instrumental detection limit of the EPMA. In the samples without a white coating (specimens YLP-3 and YLP-4), no silica precipitate was detected inside the wood cells of the sampled upper portion (c. 1 m above the ground).

In regard to the silica precipitates in the cell walls and lumina, quantitative EPMA-WDS point analysis shows that their chemical composition is constant across the cross sections of the white-coated trunks. On average, the silica precipitates consist of 88.40 wt.% SiO₂ as well as of minor amounts of Al₂O₃, CaO, Na₂O and K₂O (average 0.09, 0.19, 0.36 and 0.58 wt.%, respectively). In comparison, the silica concentration in the cell walls of the uncoated trunks is below the detection limit.

As mentioned above, silica sphere aggregates have a preference for infilling parenchyma rays and latewood lumina throughout the cross section, irrespective of their vertical position in the tree. Apart from more silica in the latewood than in the earlywood lumina, there are no differences in the quantity of other minerals in the cross sectional samples of the trunks, indicating an equal distribution of these phases throughout the length of the trunks. The consistently higher ratio in silica content between the earlywood and latewood in the lower sections of the trunks decreases toward the tree apex in the whitecoated saplings.

DISCUSSION

The extensive high-resolution mineralogical analysis of wood from lodgepole pine saplings rooted on a sinter apron offers insight into the incipient silicification of trees growing in a silica-rich, hot-spring environment with regard to the speed, mineral characterization, and physical pathway of silicification in the trees. The collecting of wood specimens with and without a white surface coating on the trunk, as well as the analysis of samples taken at different heights of the trunks, set up comparative experiments to test for incipient mineralization. Analyses by EPMA, SEM, CHRS and XRPD reveal that this white surface coating is dominated by precipitates of amorphous silica, along with minor amounts of halite and gypsum.

Cellular pathways

A major outcome of these analyses is that only when silica is found on the surface of the trunk, it will be found in the wood cells at the same height inside the trunk. In trunks without any white surface coating, any silica

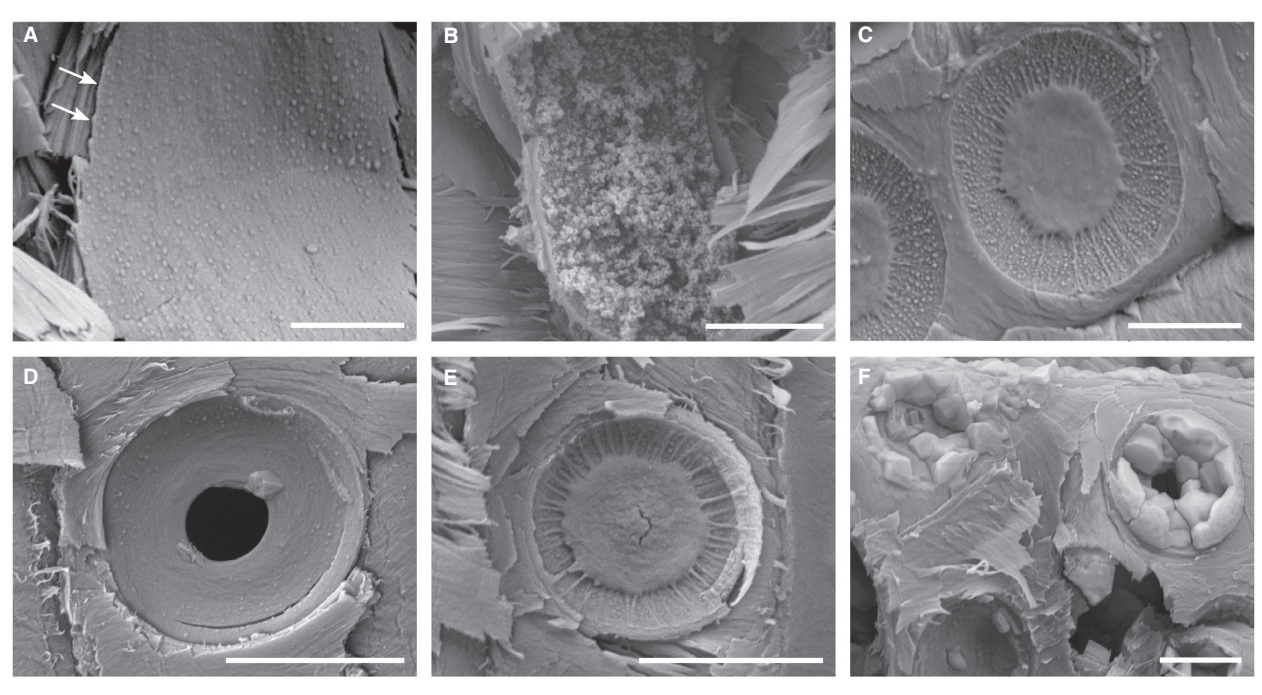


FIG. 3. Secondary electron micrographs of amorphous silica and halite micromorphology in tracheids and circular bordered pits in cross sections of lodgepole pine specimens YLP-1 and YLP-2. A, inner cell wall of an earlywood tracheid in the base of YLP-1; a dense amorphous silica layer (*c*. 400 nm; arrows) and non-uniform spheres (180–300 nm-sized) cover the cell wall. B, latewood tracheid filled with irregularly-arranged silica spheres (150–330 nm) in the lower section of YLP-2. C, circular bordered pits with torus and silica spheres covering the margo between radial microfibrils in the lower section of YLP-2. D, circular bordered pit with minor, non-uniform silica spheres and a halite cube on the pit aperture, in the apex of YLP-2; the sphere size distribution is the same as in base sections. E, circular bordered pit of the apex section of YLP-1; compared to base cross sections, silica is absent from the cell wall surface; only a few silica spheres are located between margo strands. F, halite fills the circular bordered pits, replicating the pit chamber geometry in the base section of YLP-1. Scale bars represent 10 μm.

within the wood was below the instrumental detection limits. Thus, the point of entry for aqueous silica into the young trees was generally through their periphery. The preferential silica deposition sites inside surface-coated saplings are the pit chambers, latewood tracheids, and rays. Silica precipitates in desiccation cracks and randomly distributed insect bore holes suggest that the saplings under study were at least partially decorticated prior to silicification.

It is likely that the entry of mineral-rich solution into the trees began as a result of an intensive, but short-lived discharge of oxidizing, alkali–chloride–sulphate waters in 1966 (White *et al.* 1988; Guidry & Chafetz 2002). At the collecting site (10 m from the vent), the temperature of the hot-spring waters was *c.* 50°C at a pH value *c.* 6.6 (calculated from Guidry & Chafetz 2002). It is likely that the inundation killed the trees, presumably in its flowpath, within a short period of time. During the retreat, cooling and evaporation of the bulk floodwater, the ion concentration progressively increased (Guidry & Chafetz 2002), inducing a top to bottom increase of supersaturation of the flood waters with respect to silica, halite and

gypsum. This resulted in a continuous increase in both the silica quantity inside the saplings and the thickness of the surface precipitate toward the bottom part of the saplings.

One potential pathway for silica-rich fluid to enter a rooted tree is the in vivo uptake via evapotranspiration or capillary draw soon after the plant's death (Jones et al. 1998; Channing & Edwards 2009; Ballhaus et al. 2012). As hydraulic conductivity is proportional to the fourth power of xylem conduit radius (Domec & Gartner 2002), it can be expected that the ratio between silica abundance in large earlywood tracheids and narrow latewood tracheids increases in the vertical direction. This is at odds with our general observation that silica sphere accumulations occur predominantly in the latewood lumina. The systematic positive correlation of external and internal silica abundance shows that the potential uptake of silicarich fluid by evapotranspiration or capillary action is limited to surface-coated regions and is of negligible importance over a distance greater than perhaps a few tens of centimetres, despite the abundant silica supply provided by Cistern Spring waters. Conclusively, transport of silica-

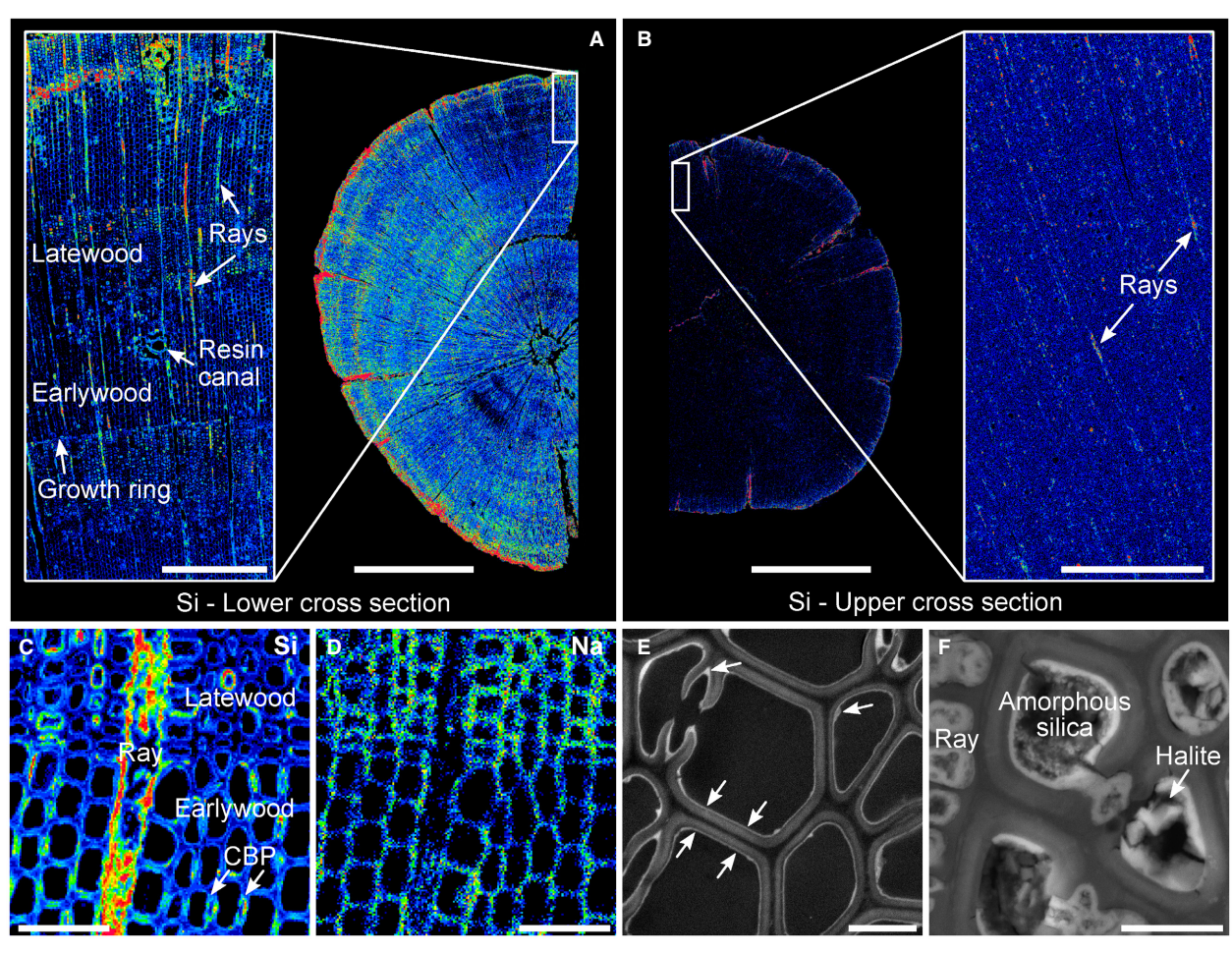


FIG. 4. EPMA wavelength-dispersive spectrometer (WDS) x-ray count maps for Si and Na and backscattered electron (BSE) images of amorphous silica precipitates in the lower cross section of specimen YLP-1. A-B, silicon distribution maps of lower (A) and upper (B) cross sections; silicon is enriched in the surface coating, latewood lumina, and rays of the lower section; the Si concentration decreases toward the top of the sapling with preferential deposition in the surface coating and rays. C-D, Si (C) and Na (D) concentration maps across a growth ring illustrate the homogeneous ion infiltration into cell walls that trace the cellular structure; silicon is enriched in the parenchyma ray and small pore spaces of latewood lumina and circular bordered pits (CBP). E, BSE image of earlywood tracheids; arrows highlight the dense amorphous silica layer on inner cell walls and pit chambers. F, BSE image of silica sphere aggregates (amorphous silica) and euhedral halite in latewood tracheids and a ray. Scale bars represent: 5 mm (A, B); 500 μm (magnified element maps: A, B); 50 μm (C, D); 10 μm (E, F).

rich fluid by evapotranspiration or capillary draw plays an insignificant role in the silicification process of lodgepole pine rooted in growth position.

After floodwater retreat, hot-spring fluid accumulates in pore space as capillary water and is held against gravity. Within a growth ring, latewood has a higher water storage capacity than earlywood due to its narrower tracheid diameter (Domec & Gartner 2002). Therefore, latewood cells and small pore spaces (e.g. pit chambers) hold fluid more tightly against gravity and are preferred sites for longitudinal fluid retention. Conversely, in horizontal orientation, the radially oriented parenchyma rays most efficiently retain silica-rich fluid. Therefore, preferential silica deposition in the parenchyma rays persists even in

the uppermost sample sections. Our observations suggest that localized fluid retention capability controls the in situ silicification process after short-term immersion in hotspring water.

The intraplant precipitation of amorphous silica has frequently been attributed to the decomposition of organic tissue, resulting in acidification of the fluid, decrease in silica solubility, and localized silica nucleation and growth (Leo & Barghoorn 1976; Jones et al. 1998; Ballhaus et al. 2012). However, in the circumneutral alkali-chloride-sulphate Cistern Spring fluids (Guidry & Chafetz 2002), the pH decrease associated with plant material decomposition does not lower the solubility of amorphous silica (Iler 1979). The silica solubility in the

658 PALAEONTOLOGY, VOLUME 63

Cistern Spring waters also remains constant in the pH range of conifer xylem water (pH c. 5.5–7.5; see Marschner 1995; Losso et al. 2018). Thus, it is unlikely that silica precipitation in Cistern Spring saplings resulted from the mixing of xylem water with circumneutral spring fluid or a pH gradient created by organic substance degradation. It is more likely that the silica precipitation process proceeds via the initial interaction with the organic substrate and subsequent formation of characteristic growth morphologies, which is dependent on dissolved silica concentration.

Internally retained floodwater forms a fluid film adhering to cell walls (Fig. 5). Silica deposition begins on the inner cell wall and potentially at intracellular hydroxyl groups of lignin and holocellulose molecules (Sigleo 1978; Jefferson 1987; Perry & Lu 1992). The lack of significant ion impurities in the lignin-rich cell components reflects their hydrophobic character and smaller swelling capacity (Panshin et al. 1964; Maloney & Paulapuro 1999). Analogous to microorganisms (Alleon et al. 2016), the entombment of plant organic substance with amorphous silica may limit its degradation. Initially, silica monomer attachment to hydroxyl groups of the cell wall surface results in a silica monolayer. When the inner cell wall is covered with this early-stage monolayer, further aqueous silica (monomeric or simple polymeric) forms siloxane bonds with the previous accumulations. The still high level of supersaturation with respect to amorphous silica results in rapid precipitation of the up to 800 nm-thick dense layer at a high polymerization rate (Van den Heuvel et al. 2018). The thickness of these silica films is comparable to those developed in herbaceous plants cyclically (in experiments lasting 11 months) or continuously (duration unknown) immersed in hot-spring water (Channing & Edwards 2003, 2009). However, compared to herbaceous plants, the ratio of silica films to spheres in lodgepole pine saplings is substantially higher.

The change of the silica micromorphology from a dense layer to single spheres shows that precipitation efficiently reduces the silica concentration in the fluid film. Cooling-related silica precipitation alone would result in a continuous increase of amorphous silica saturation (Guidry & Chafetz 2002) and, accordingly, a reverse order in precipitate morphology. At sufficiently low silica concentration, the formation and growth of large particles dominates, resulting in c. 150-350 nm-sized, non-uniform spheres with similar size distribution throughout the samples. In contrast to formation in dense films, these spheres form at lower levels of supersaturation and a lower polymerization rate. The resulting spheres move as free units in a sol and attach to previously deposited silica layers due to their attractive interaction potential. We expect that the solution composition is similar on both sides of the dense silica layer (i.e. in cell walls and

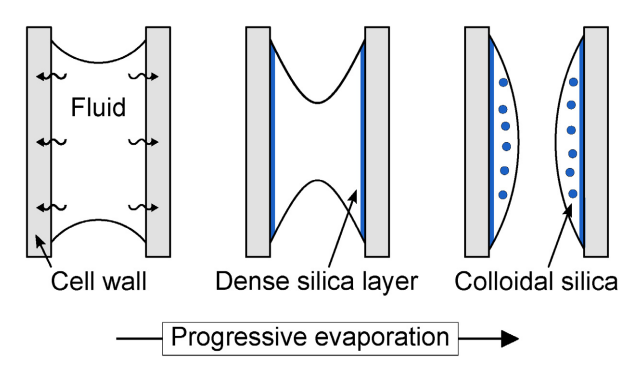


FIG. 5. Schematic representation of the micromorphological changes of non-crystalline silica during fluid evaporation. Dissolved silica enters the cell wall and initially bonds to the hydroxyl groups of the organic substrate. Later, dissolved silica in the fluid film forms siloxane bonds with this precipitate. As the silica concentration in the fluid decreases, colloidal spheres form and attach to the previously formed dense silica layer. Colour online.

lumina). Therefore, spheres in cell walls may also form at comparably low silica concentration. Residual aqueous silica can bond to available silica surfaces and remaining organic reactive surface sites.

A rapid pace of silicification

Element distribution mapping shows that inorganic impurities in cell walls evenly reflect the cellular structure, implying rapid fluid migration into the swollen organic substrate. This observation indicates that inner cell wall coating and cell wall impregnation by amorphous silica occurred simultaneously. The structural and chemical homogeneity of amorphous silica and the absence of a radial concentration gradient toward the centre of the woody axis suggest that the fluid composition remained constant during infiltration.

The white silica-halite-gypsum surface precipitate on the saplings and on all surrounding trees at the same height (c. 0.8 m) implies that flooding and subsequent mineral precipitation affected plant material in growth position simultaneously. However, no long-lasting flooding has been reported for the closely monitored Cistern Spring study area since spring activity in 1966 (White et al. 1988; Fournier 1989; Fournier et al. 1994). Thus, vent fluid enclosed the saplings for no longer than perhaps a few days or weeks in 1966. Apparently, all the silicification took place within this short time span. This implies that in situ plant silicification by permineralization is a very rapid process that takes only days or weeks rather than requiring months or years, as has been previously suggested based on taphonomic experiments conducted in hot-spring settings (Channing & Edwards 2003, 2009).

Fossilization potential

Based on our analytical data, the fossilization potential of trees rooted in a hot-spring environment can be addressed. Halite precipitation and growth inside cell walls results in partial destruction by the force of crystallization. Accordingly, wetting-drying cycles significantly lower the potential for cell preservation. Prolonged immersion may have also overprinted possible evidence of spatially selective silicification, for example, inwardmoving fronts of silicification (Channing & Edwards 2003). Interestingly, previous studies on cyclically immersed, above-ground plant material in Yellowstone hot-spring settings do not show evidence for precipitates other than silica (e.g. Channing & Edwards 2003). The absence of crystallization pressure may be fundamental for the exceptional preservation of cell wall structure and organic components (e.g. Strullu-Derrien et al. 2019) during amorphous silica precipitation and throughout the diagenetic transformation to crystalline silica phases. An additional silica supply is crucial for the volume-preserving replacement of plant material on the amorphous-tocrystalline pathway toward more ordered opal phases and quartz. Otherwise, silica re-crystallization may result in substantial volume reduction and collapse of cellular structure. The aerial silica-halite-gypsum surface precipitate on the saplings studied here effectively stabilizes the plant material against collapse.

CONCLUSIONS

X-ray powder diffraction, Raman spectroscopy, scanning electron microscopy, and electron probe microanalysis indicate the absence of a preferential pathway of silicarich fluid into short-termed waterlogged pine trees in growth position. In fact, the preferential fluid retention in small pore space controls the silicification process during evaporative ion concentration. The distinct coupling of the silica quantity inside and on the surface of the saplings provides evidence for the negligible contribution of capillary draw or in vivo fluid uptake to pine silicification.

From our observations, we conclude that in situ plant permineralization by silicification is a fast process, occurring within days to weeks rather than several months or years. Our analytical results show that short-term immersion in hot-spring water results in concurrent cell wall accumulation with amorphous silica layers and cell wall infiltration with hot-spring fluid. The inorganic ion impurity distribution implies that cell wall composition (cellulose-rich vs lignin-rich) has the largest impact on fluid infiltration into the cell wall, irrespective of cell type or position within the sapling. Swelling of the cell wall

facilitates the infiltration process without the need for plant material degradation. We attribute the systematic shift in amorphous silica micromorphology (from dense layers to spheres) to the coupled decrease of dissolved silica concentration and polymerization rate in the continuously evaporating fluid film on the cell wall surface.

Acknowledgements. Funding for this research was provided by grant GE 751/5-1 from the German Research Council (Deutsche Forschungsgemeinschaft) to Carole T. Gee. We sincerely thank the Editor Leyla Seyfullah, Sally Thomas (Palaeontological Association) and an anonymous reviewer for their detailed and thoughtful comments. We thank Martina Menneken for assistance with the Raman spectrometer at the University of Bonn, Timm John for access to x-ray diffraction facilities at the Freie Universität Berlin (Germany), as well as Martin Sander and Martin Schilling for their support. We gratefully acknowledge Yellowstone National Park permit number YELL-2011-SCI-5912. This is contribution no. 13 of the DFG Research Unit FOR 2685 'The limits of the fossil record: Analytical and experimental approaches to fossilization'.

REFERENCES

- ALLEON, J., BERNARD, S., LE GUILLOU, C., DAVAL, D., SKOURI-PANET, F., PONT, S., DELBES, L. and ROBERT, F. 2016. Early entombment within silica minimizes the molecular degradation of microorganisms during advanced diagenesis. Chemical Geology, 437, 98-108.
- BALLHAUS, C., GEE, C. T., BOCKRATH, C., GREEF, K., MANSFELDT, T. and RHEDE, D. 2012. The silicification of trees in volcanic ash—an experimental study. Geochimica et Cosmochimica Acta, 84, 62-74.
- BECK, C. B. 1960. The identity of Archaeopteris and Callixylon. Brittonia, 12, 351-368.
- CHANNING, A. and EDWARDS, D. 2003. Experimental taphonomy: silicification of plants in Yellowstone hot-spring environments. Earth & Environmental Science Transactions of the Royal Society of Edinburgh, 94 (4), 503-521.
- 2009. Silicification of higher plants in geothermally influenced wetlands: Yellowstone as a Lower Devonian Rhynie analog. Palaios, 24, 505-521.
- DOMEC, J.-C. and GARTNER, B. L. 2002. How do water transport and water storage differ in coniferous earlywood and latewood? Journal of Experimental Botany, 53, 2369-2379.
- EDWARDS, D., KENRICK, P. and DOLAN, L. 2017. History and contemporary significance of the Rhynie cherts our earliest preserved terrestrial ecosystem. Philosophical Transactions of the Royal Society B, 373, 20160489.
- FOURNIER, R. O. 1989. Geochemistry and dynamics of the Yellowstone National Park hydrothermal system. Annual Review of Earth & Planetary Sciences, 17, 13-53.
- CHRISTIANSEN, R. L., HUTCHINSON, R. A. and PIERCE, K. L. 1994. A field-trip guide to Yellowstone National Park, Wyoming, Montana, and Idaho - volcanic, hydrothermal, and glacial activity in the region. US Geological Survey Bulletin, **2099**, 1–46.

- GÖTZE, J., PLÖTZE, M. and HABERMANN, D. 2001. Cathodoluminescence (CL) of quartz: origin, spectral characteristics and practical applications a review. *Mineralogy & Petrology*, 71, 225–250.
- GRAETSCH, H. 1994. Structural characteristics of opaline and microcrystalline silica minerals. 209–232. *In* HEANEY, P. J., PREWITT, C. T. and GIBBS, G. V. (eds). *Silica: Physical behavior, geochemistry, and materials applications*. Reviews in Mineralogy, 29, Mineralogical Society of America, 606 pp.
- GUIDRY, S. A. and CHAFETZ, H. S. 2002. Factors governing subaqueous siliceous sinter precipitation in hot springs: examples from Yellowstone National Park, USA. *Sedimentology*, **49**, 1253–1267.
- HELLAWELL, J., BALLHAUS, C., GEE, C. T., MUSTOE, G. E., NAGEL, T. J., WIRTH, R., RETHE-MEYER, J., TOMASCHEK, F., GEISLER, T., GREEF, K. and MANSFELDT, T. 2015. Incipient silicification of recent conifer wood at a Yellowstone hot spring. *Geochimica et Cosmochimica Acta*, 149, 79–87.
- HEUVEL, D. B. VAN DEN, GUNNLAUGSSON, E., GUNNARSSON, I., STAWSKI, T. M., PEACOCK, C. L. and BENNING, L. G. 2018. Understanding amorphous silica scaling under well-constrained conditions inside geothermal pipelines. *Geothermics*, 76, 231–241.
- ILER, R. K. 1979. The Chemistry of silica: Solubility, polymerization, colloid and surface properties, and biochemistry. Wiley, 896 pp.
- JEFFERSON, T. H. 1987. The preservation of conifer wood: examples from the Lower Cretaceous of Antarctica. *Palaeontol-ogy*, 30, 233–249.
- JONES, J. B. and SEGNIT, E. R. 1971. The nature of opal I. Nomenclature and constituent phases. *Journal of the Geological Society of Australia*, 18, 37–41.
- JONES, B., RENAUT, R. W., ROSEN, M. R. and KLYEN, L. 1998. Primary siliceous rhizoliths from Loop Road hot springs, North Island, New Zealand. *Journal of Sedimentary Research*, 68, 115–123.
- LEO, R. F. and BARGHOORN, E. S. 1976. Silicification of wood. *Harvard University Botanical Museum Leaflets*, **25**, 1–47.
- LIESEGANG, M. and MILKE, R. 2018. Silica colloid ordering in a dynamic sedimentary environment. *Minerals*, 8, 12.
- KRANZ, C. and NEUSSER, G. 2017. Silica nanoparticle aggregation in calcite replacement reactions. Scientific Reports, 7, 14550.
- and BERTHOLD C. 2018. Amorphous silica maturation in chemically weathered clastic sediments. *Sedimentary Geology*, **365**, 54–61.
- LOSSO, A., NARDINI, A., DÄMON, B. and MAYR, S. 2018. Xylem sap chemistry: seasonal changes in timberline

- conifers Pinus cembra, Picea abies, and Larix decidua. Biologia Plantarum. **62**, 157–165.
- MALONEY, T. C. and PAULAPURO, H. 1999. The formation of pores in the cell wall. *Journal of Pulp & Paper Science*, **25**, 430–436.
- MARSCHNER, H. 1995. Mineral nutrition of higher plants. 2nd edn. Academic Press, 889 pp.
- McMILLAN, P. 1984. Structural studies of silicate glasses and melts-applications and limitations of Raman spectroscopy. American Mineralogist, 69, 622–644.
- MURATA, K. 1940. Volcanic ash as a source of silica for the silicification of wood. *American Journal of Science*, **238**, 586–596.
- PANSHIN, A. J., ZEEUW, C. DE and BROWN, H. P. 1964. Textbook of wood technology. Vol. 1: Structure, identification, uses, and properties of the commercial woods of the United States. 2nd edn. McGraw-Hill, 643 pp.
- PERRY, C. C. and LU, Y. 1992. Preparation of silicas from silicon complexes: role of cellulose in polymerisation and aggregation control. *Journal of the Chemical Society, Faraday Transactions*, 88, 2915–2921.
- RODGERS, K. A., BROWNE, P. R. L., BUDDLE, T. F., COOK, K. L., GREATREX, R. A., HAMPTON, W. A., HERDIANITA, N. R., HOLLAND, G. R., LYNNE, B. Y., MARTIN, R., NEWTON, Z., PASTARS, D., SANNAZARRO, K. L. and TEECE, C. I. A. 2004. Silica phases in sinters and residues from geothermal fields of New Zealand. *Earth-Science Reviews*, **66**, 1–61.
- SIGLEO, A. C. 1978. Organic geochemistry of silicified wood, Petrified Forest National Park, Arizona. Geochimica et Cosmochimica Acta, 42, 1397–1405.
- STRULLU-DERRIEN, C., BERNARD, S., SPENCER, A. R., REMUSAT, L., KENRICK, P. and DERRIEN, D. 2019. On the structure and chemistry of fossils of the earliest woody plant. *Palaeontology*, **62**, 1015–1026.
- TRÜMPER, S., RÖßLER, R. and GÖTZE, J. 2018. Deciphering silicification pathways of fossil forests: case studies from the late Paleozoic of Central Europe. *Minerals*, **8**, 432.
- WALLER, J., BLACKFORD, T. and YOUNG, L. 2019. Vegetation. 143–159. *Yellowstone resources and issues handbook*. Yellowstone National Park, WY. 304 pp.
- WHITE, D. E., HUTCHINSON, R. A. and KEITH, T. E. C. 1988. The geology and remarkable thermal activity of Norris Geyser Basin, Yellowstone National Park, Wyoming. *United States Geological Survey Professional Paper*, **1456**, 84 pp.
- XU, H.-H., BERRY, C. M., STEIN, W. E., WANG, Y., TANG, P. and FU, Q. 2017. Unique growth strategy in the Earth's first trees revealed in silicified fossil trunks from China. *Proceedings of the National Academy of Sciences*, 114, 12009–12014.